Acta Mech 229, 2719–2735 (2018)
https://doi.org/10.1007/s00707-018-2135-1

CrossMark

ORIGINAL PAPER

Qing Chen · Hehua Zhu · J. Woody Ju · Zhiguo Yan · Changhong Wang · Zhengwu Jiang

A stochastic micromechanical model for fiber-reinforced concrete using maximum entropy principle

Received: 10 July 2017 / Revised: 29 January 2018 / Published online: 8 March 2018

Abstract A stochastic micromechanical framework is presented to predict the probabilistic behavior of the fiber-reinforced concrete (FRC) using the maximum entropy principle. The FRC is represented as a multiphase composite composed of the aggregate, the interfacial transition zone, the bulk cement paste, and the fiber. The volume fractions of the different constituents are analytically calculated based on the material mix proportions and the aggregate grading. The multilevel homogenization schemes are presented to predict the material's effective properties considering the effects of the aggregate, the ITZ, and the fibers with the different shapes. By modeling the volume fractions and properties of constituents as stochastic, we extend the deterministic framework to stochastic to incorporate the inherent randomness of effective properties among the different specimens. The maximum entropy distribution is modified to estimate the probability density function of the material's properties using their different order moments. Numerical examples including the limited experimental validations, the comparisons with existing micromechanical models, the commonly used probability density functions, and the direct Monte Carlo simulations indicate that the proposed models provide an accurate and computationally efficient framework in characterizing the material's effective properties.

Q. Chen (✉)· Z. Jiang (✉)
Key Laboratory of Advanced Civil Engineering Materials (Tongji University), Ministry of Education,
4800 Cao'an Road, Shanghai 201804, China
E-mail: chenqing19831014@163.com

Z. Jiang
E-mail: jzhw@tongji.edu.cn

Q. Chen
Shaanxi Provincial Major Laboratory for Highway Bridge and Tunnel, Chang'an University, Xi'an 710064, Shaanxi, China

H. Zhu · Z. Yan
State Key Laboratory for Disaster Reduction in Civil Engineering, Tongji University, 1239 Siping Road, Shanghai 200092, China

H. Zhu · Z. Yan
Key Laboratory of Geotechnical and Underground Engineering of the Ministry of Education, Tongji University, 1239 Siping Road, Shanghai 200092, China

J. W. Ju
Department of Civil and Environmental Engineering, University of California, Los Angeles, CA 90095, USA

C. Wang (✉)
Department of Civil Engineering, Shanghai Univesitiy, 99 Shangda Road, Shanghai 200444, China
E-mail: changhong.wangsir@gmail.com

1 Introduction

Owing to the well-established performance of the fiber-reinforced concrete (FRC), major efforts have been dedicated during the last decade to the modeling of the material's behavior [1–8]. The empirical formulations to evaluate the elastic properties of FRC have been suggested by many researches [6–9]. These formulations are usually obtained by means of the laboratory tests, which is the phenomenological way to formulate the behavior of the FRC. An attractive alternative to handle this kind of problem is provided by the framework of micromechanics, which reduces the laboratory expenses, meanwhile discloses the enhancing mechanism of the fibers from the microscale level [10–13]. Teng et al. [11] proposed a dedicated empirical formula for calculating the elastic moduli of steel fiber-reinforced concrete (SFRC) by adopting the equivalent inclusion method. Dutra et al. [10] proposed a micromechanical model for the FRC, and the linear elastic behavior is examined by implementation of a Mori-Tanaka homogenization scheme. Gal and Kryvoruk [12] employed the finite element method to analyze the properties of FRC using a two-step homogenization approach, where the *interfacial transition zone* (ITZ) between the aggregate and mortar is considered by a micromechanical homogenization process. Guan et al. [13] presented a stochastic micromechanical model to characterize the elastic modulus and Poisson's ratio of FRC.

It is indeed effective and promising to use the micromechanics to predict the behavior of FRC. However, very few models considering the effects of both the ITZ and fiber shapes together are available according to the present studies on the micromechanical modeling for the FRC [10–13]. Furthermore, the current micromechanical models for the FRC are mainly based on the deterministic micromechanical framework which does not consider the stochastic behavior of composites observed in the actual specimens [14–22]. Due to the difficulties in detailing the exact pre-determined microstructural composites, there is an inherent randomness of the microstructures even under the same manufacturing process [14–16]. To address these shortcomings, a deterministic micromechanical framework is proposed for FRC considering the influence of aggregate grading, the ITZ, and fibers with different shapes in this paper. Meanwhile, by modeling the volume fractions and properties of constituents as stochastic, the deterministic framework is extended to stochastic to incorporate the inherent randomness of the effective properties among the different specimens. Furthermore, the efficient simulation program based on the maximum entropy principle is presented to obtain the unbiased probability density function of the FRC's properties.

The rest of this paper is organized as follows. The maximum entropy distribution is introduced in Sect. 2. Section 3 proposes the deterministic micromechanical framework for the FRC, which includes the material's multiphase micromechanical model, the multilevel homogenization scheme for predicting the FRC's effective properties, and the analytical solutions for the volume fractions of the different constituents (consisting of the aggregate, the ITZ, the bulk cement paste, and the fibers with different shapes). In Sect. 4, stochastic micromechanical framework for the FRC is obtained by modeling the properties and the volume fractions of the constituents as stochastic. Meanwhile, the moments of the effective properties are calculated with Monte Carlo simulations, with which the maximum entropy distribution is modified to estimate the probability density function (pdf) of the material's properties. Numerical examples including validations and discussions are presented in Sect. 5. And some conclusions are reached in the final Section.

2 Maximum entropy distribution

2.1 The maximum principle

In information theory, the entropy is a measure of the uncertainty associated with a random variable. It can be defined as

$$H(x) = -\int_{-\infty}^{\infty} f(x) \ln[f(x)]\mathrm{d}x \tag{1}$$

where $H(x)$ is the entropy and $f(x)$ is the pdf of a random variable x. The maximum entropy principle was developed by Jaynes on the basis of the concept of the statistical entropy, which can be viewed as a rational approach for choosing a consistent probability distribution among all possible distributions [23]. The principle states that the minimally prejudiced probability distribution is the one that maximizes the entropy subject to the constraints.

2.2 The maximum entropy distribution

Let us define the normalization condition and moments as below, which can be seen as the constraints for the pdf of a random variable,

$$\int_{-\infty}^{\infty} f(x)\mathrm{d}x - 1 = 0, \tag{2}$$

$$\int_{-\infty}^{\infty} x^i f(x)\mathrm{d}x - m_i = 0 \tag{3}$$

where m_i is the i-order moment of the random variable.

To obtain the maximum entropy distribution, the Euler–Lagrange equation can be applied to solve the function maximum problem, and the solution is

$$f(x) = \exp\left[\mathrm{a}_0 + \sum_{i=1}^{N} a_i x^i\right] \tag{4}$$

where $a_0, a_1, a_2, \cdots a_N$ are the Lagrangian multipliers [24].

By differentiating the definition of the maximum entropy distributions with respect to the variable x, we have

$$f'(x) = \left(\sum_{i=1}^{N} a_i x^{i-1}\right) f(x). \tag{5}$$

If we multiply both sides of Eq. (5) by x^n (n is a positive integer) and perform the integration with respect to x, the Lagrangian multipliers $a_1, a_2, \cdots a_N$ can be obtained after lengthy derivations by solving the following equations [24]:

$$\begin{pmatrix} 1 & m_1 & m_2 & \cdots & m_{N-1} \\ m_1 & m_2 & m_3 & \cdots & m_N \\ m_2 & m_3 & m_4 & \cdots & m_{N+1} \\ \vdots & \vdots & \vdots & \ddots & \vdots \\ m_{N-1} & m_N & m_{N+1} & \cdots & m_{2N-2} \\ m_N & m_{N+1} & m_{N+2} & \cdots & m_{2N-1} \\ m_{N+1} & m_{N+2} & m_{N+3} & \cdots & m_{2N} \\ & & \vdots & & \end{pmatrix} \begin{pmatrix} a_1 \\ 2a_2 \\ 3a_3 \\ \vdots \\ Na_N \end{pmatrix} = \begin{pmatrix} 0 \\ -1 \\ -2m_1 \\ \vdots \\ -(N-1)m_{N-2} \\ -Nm_{N-1} \\ -(N+1)m_N \\ \vdots \end{pmatrix}. \tag{6}$$

With $a_1, a_2, \cdots a_N$, the parameter a_0 can be reached using the normalization condition as below:

$$a_0 = \ln\left(\frac{1}{\int_{-\infty}^{+\infty} \exp\left[\sum_{i=1}^{N} a_i x^i\right]}\right). \tag{7}$$

3 Deterministic micromechanical framework for the FRC

3.1 Multiphase micromechanical model for the FRC

The FRC can be seen as the composite composed by the concrete and the fibers. It is complicated and often impossible to precisely describe the concrete's microstructures. There are many different constituents in the concrete at the different length scales [25–30]. The concrete can be treated as homogenous material at the macroscopic scale. At the lower level, the material is made of the aggregates (rock and sand), the cement

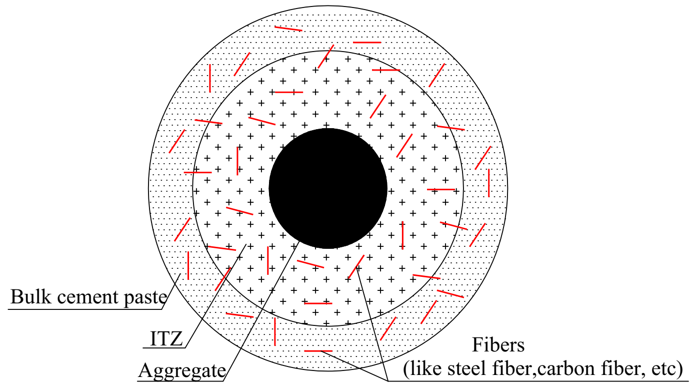

Fig. 1 Multiphase micromechanical model for fiber-reinforced concrete (FRC)

pastes, and the ITZs. The cement pastes are formed by the homogeneous C–S–H with the large CH crystals, the aluminates, the cement clinker and the water; and the microstructures of the ITZs are much more complex [25,26]. In this paper, following the previous works [27–29], the shape of the aggregate is supposed to be spherical. As regards the shape of each fiber, it is characterized by the aspect ratio $\gamma = a/b$. Note that the scalars a and b refer, respectively, to the semimajor axis and to the semiminor axis of the representing prolate spheroid for a fiber. Furthermore, the interface between the fiber and matrix is assumed to be well bonded [10–13]. Therefore, to investigate the effects of the fibers with different shapes and the ITZs on the FRC properties, the material in this paper is described as four-phase composite composed of the fiber, the bulk cement phase, the aggregates (sand and rock), and the ITZ between them [10–13,27–29], as shown in Fig. 1.

3.2 Multilevel homogenization scheme for the effective properties of the FRC

Previously published studies have shown that a homogenization stepping scheme is an effective way to obtain the effective properties of the multi-inclusion composites [31–54]. The multiphase micromechanical model used in the present study also employs a multilevel homogenization procedure. First, the equivalent inclusion (composed of the aggregate and the ITZ) and the equivalent matrix (i.e., concrete) are reached by modifying the three-phase sphere model presented by Smith in the first and second-level homogenizations [55,56], as shown in Fig. 2a, b. Second, the fibers with different shapes are incorporated by utilizing the work of Berryman in the third-level homogenization [57], as exhibited in Fig. 2c.

3.2.1 The effective properties of the composite made up of the aggregate and the ITZ

The first-level homogenization employs the three-phase sphere model to obtain the effective bulk modulus and the effective shear modulus of the equivalent inclusion. For the two-phase composite made up of the aggregates (as the inner material) and the ITZ (as the outer material), the effective properties can be reached based on [55,56], which can be expressed as below:

$$K_F = K_{\text{itz}} + \frac{\phi_{\text{ag}}\left(K_{\text{ag}} - K_{\text{itz}}\right)\left(3K_{\text{itz}} + 4\mu_{\text{itz}}\right)}{3K_{\text{itz}} + 4\mu_{\text{itz}} + 3\left(1-\phi_{\text{ag}}\right)\left(K_{\text{ag}} - K_{\text{itz}}\right)}, \tag{8}$$

$$\alpha\left(\frac{\mu_F}{\mu_{\text{itz}}} - 1\right)^2 + \beta\left(\frac{\mu_F}{\mu_{\text{itz}}} - 1\right) + \gamma = 0. \tag{9}$$

With

$$\phi_{\text{ag}} = \frac{c_{\text{ag}}}{c_{\text{ag}} + c_{\text{itz}}}, \tag{10}$$

$$\alpha = [4P(7 - 10\nu_{\text{itz}}) - S\phi_{\text{ag}}^{7/3}][Q - (8 - 10\nu_{\text{itz}})(M-1)\phi_{\text{ag}}] \\ -126P(M-1)\phi_{\text{ag}}\left(1 - \phi_{\text{ag}}^{2/3}\right)^2, \tag{11}$$

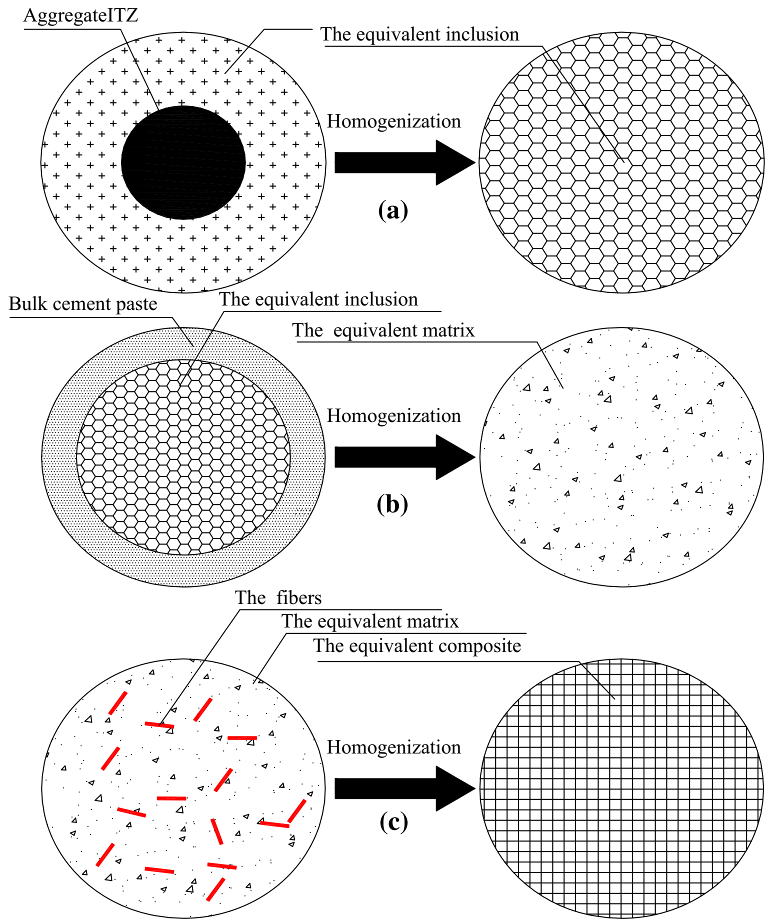

Fig. 2 The multilevel homogenization procedures: **a** the first-level: homogenization of the aggregate and ITZ; **b** the second-level: homogenization of the bulk cement paste and equivalent inclusion; **c** the third-level: homogenization of the equivalent matrix and the fibers

$$\beta = 35(1-\nu_{\text{itz}})P[Q-(8-10\nu_{\text{itz}})(M-1)\phi_{\text{ag}}] \\ -15(1-\nu_{\text{itz}})[4P(7-10\nu_{\text{itz}})-S\phi_{\text{ag}}^{7/3}](M-1)\phi_{\text{ag}}, \tag{12}$$

$$\gamma = -525P(1-\nu_{\text{itz}})^2(M-1)\phi_{\text{ag}}, \tag{13}$$

$$M = \frac{\mu_{\text{ag}}}{\mu_{\text{itz}}}, \tag{14}$$

$$P = (7+5\nu_{\text{ag}})M + 4(7-10\nu_{\text{ag}}), \tag{15}$$

$$Q = (8-10\nu_{\text{itz}})M + (7-5\nu_{\text{itz}}), \tag{16}$$

$$S = 35(7+5\nu_{agg})M(1-\nu_{\text{itz}}) - P(7+5\nu_{\text{itz}}) \tag{17}$$

where K_F and μ_F are the effective bulk modulus and shear modulus of the equivalent inclusions after the first-level homogenization, ϕ_{ag} is the volume fractions of the aggregates in the two-phase composite made up of the aggregate and the ITZ, c_{ag} and c_{itz} are the volume fractions of the aggregate and the ITZ; K_{ag}, μ_{ag} and ν_{ag}(K_{itz}, μ_{itz} and ν_{itz}) are the bulk modulus, the shear modulus, and Poisson's ratio for the aggregates (the ITZ).

3.2.2 The effective properties of the concrete

As to the concrete consisting of the bulk cement paste and the equivalent inclusion, the material's effective mechanical properties can be similarly obtained by employing the three-phase sphere model of Smith [55,56]. Let K_{bk}, μ_{bk} and ν_{bk} signify the bulk modulus, the shear modulus, and the Poisson's ratio of the bulk cement paste and ν_F be the effective Poisson's ratio of the equivalent inclusions. The effective properties of the three-phase composite, including the aggregates, the ITZ, and the bulk cement paste, can be reached by following alterations to Eqs. (8)–(17): firstly, K_{itz}, μ_{itz}, and ν_{itz}(K_{ag}, μ_{ag} and ν_{ag}) in Eqs. (8)–(17) should be replaced with K_{bk}, μ_{bk} and ν_{bk} (K_F, μ_F, and ν_F), respectively. Secondly, K_F and μ_F should be turned into the effective bulk modulus and shear modulus of the three-phase composite, denoted by K_S and μ_S, respectively. Thirdly, ϕ_{ag} should be replaced by ϕ_F, which can be defined by Eq. (18) as below:

$$\phi_F = \frac{c_{\mathrm{ag}} + c_{\mathrm{itz}}}{c_{\mathrm{ag}} + c_{\mathrm{itz}} + c_{\mathrm{bk}}} \tag{18}$$

where c_{bk} is the volume fraction of the bulk cement paste.

3.2.3 The effective properties of the FRC

There are usually many types of fibers, such as the steel fiber, the polypropylene fiber, and the carbon fiber, which have different shapes (characterized by the different aspect ratios). In this Section, the work of Berryman is modified to incorporate the effects of fibers with different shapes on the effective properties of the FRC [57]. By replacing the matrix phase and the inclusion phase with the concrete and the fibers, respectively, the effective properties of the FRC can be reached using the following equations [57]:

$$(K_S - K^*)\frac{K_S + (4/3)\mu_S}{K^* + (4/3)\mu_S} = c_{fi}(K_S - K_{fi})P, \tag{19}$$

$$(\mu_S - \mu^*)\frac{\mu_S + Y}{\mu^* + Y} = c_{fi}(\mu_S - \mu_{fi})Q \tag{20}$$

with

$$Y = \frac{\mu_s}{6}\frac{9K_s + 8\mu_s}{K_s + 2\mu_s} \tag{21}$$

where K_{fi} and μ_{fi} represent the bulk modulus and the shear modulus of the fiber, respectively, and c_{fi} is the volume fraction of the fiber. P and Q are related to the shape of the fiber as below:

$$P = \frac{F_1}{F_2},\ Q = \frac{2}{F_3} + \frac{1}{F_4} + \frac{F_4F_5 + F_6F_7 - F_8F_9}{F_2F_4} \tag{22}$$

with

$$F_1 = 1 + A\left[\frac{3}{2}(f+\theta) - R\left(\frac{3}{2}f + \frac{5}{2}\theta - \frac{4}{3}\right)\right], \tag{23}$$

$$F_2 = 1 + A\left[1 + \frac{3}{2}(f+\theta) - \frac{R}{2}(3f+5\theta)\right] + B(3-4R) + \frac{A}{2}(A+3B)(3-4R)\left[f+\theta-R(f-\theta+2\theta^2)\right], \tag{24}$$

$$F_3 = 1 + A\left[1 - \left(f + \frac{3}{2}\theta\right) + R(f+\theta)\right], \tag{25}$$

$$F_4 = 1 + \frac{A}{4}[(f+3\theta) - R(f-\theta)], \tag{26}$$

$$F_5 = A\left[-f + R\left(f + \theta - \frac{4}{3}\right) + B\theta(3-4R)\right], \tag{27}$$

$$F_6 = 1 + A[1 + f - R(f+\theta) + B(1-\theta)(3-4R)], \tag{28}$$

$$F_7 = 2 + \frac{A}{4}[3f + 9\theta - R(3f+5\theta) + B\theta(3-4R)], \tag{29}$$

$$F_8 = A\left[1 - 2R + \frac{f}{2}(R-1) + \frac{\theta}{2}(5R-3)\right] + B(1-\theta)(3-4R), \tag{30}$$

$$F_9 = A[(R-1)f - R\theta] + B\theta(3-4R). \tag{31}$$

The parameters A, B, and R can be arrived with the properties of the fibers and the concrete as follows:

$$A = \frac{\mu_{fi}}{\mu_S} - 1, \tag{32}$$

$$B = \frac{1}{3}\left(\frac{K_{fi}}{K_S} - \frac{\mu_{fi}}{\mu_S}\right), \tag{33}$$

$$R = \frac{3\mu_S}{3K_S + 4\mu_S}. \tag{34}$$

θ and f are defined by the following equations depending on the aspect ratios of the fiber:

$$\theta = \begin{cases} (\gamma^{-2/3} - \gamma^{4/3})^{-3/2}[\arccos\gamma - \gamma(1-\gamma^2)^{1/2}] & \gamma < 1 \\ \frac{2}{3} & \gamma = 1, \\ (\gamma^{4/3} - \gamma^{-2/3})^{-3/2}[\gamma(\gamma^2-1)^{1/2} - \operatorname{arccos} h\gamma] & \gamma > 1 \end{cases} \tag{35}$$

$$f = \begin{cases} \frac{3\theta-2}{\gamma^{-2}-1} & \gamma < 1 \\ -\frac{2}{5} & \gamma = 1 \\ \frac{2-3\theta}{1-\gamma^{-2}} & \gamma > 1 \end{cases} \tag{36}$$

where γ is the aspect ratio of the fibers.

3.3 Analytical solutions for the volume fractions of the different constituents

The volume fraction of the aggregate c_{ag} and the fiber c_{fi} can be obtained according to the mix proportions for the FRC. Since the ITZs are usually overlapped in the typical concrete, it is difficult to obtain their volume fractions. For simplicity, the volume fractions of the bulk cement phase and the ITZ are calculated by modifying the ‘void exclusion probability’ as follows [27,28,58,59]:

$$c_{\mathrm{bk}} = (1 - c_{\mathrm{ag}})\exp(-\pi\rho(\alpha t + \beta t^2 + \kappa t^3)), \tag{37}$$

$$\alpha = \frac{4\overline{R^2}}{1 - c_{\mathrm{ag}}}, \tag{38}$$

$$\beta = \frac{4\bar{R}}{1 - c_{\mathrm{ag}}} + \frac{12\varepsilon_2\overline{R^2}}{(1 - c_{\mathrm{ag}})^2}, \tag{39}$$

$$\kappa = \frac{4}{3(1 - c_{\mathrm{ag}})} + \frac{8\varepsilon_2\bar{R}}{(1 - c_{\mathrm{ag}})^2}, \tag{40}$$

$$\varepsilon_2 = \frac{2\pi\rho\overline{R^2}}{3}, \tag{41}$$

$$\rho = \sum_{i=1}^{Nu}\frac{9c_{\mathrm{ag}}c_i}{4\pi\left(r_{i+1}^3 - r_i^3\right)}\ln\left(\frac{r_{i+1}}{r_i}\right), \tag{42}$$

$$\bar{R} = \sum_{i=1}^{Nu}\frac{9c_{\mathrm{ag}}c_i}{4\pi\rho\left(r_{i+1}^3 - r_i^3\right)}(r_{i+1} - r_i), \tag{43}$$

$$\overline{R^2} = \sum_{i=1}^{Nu}\frac{9c_{\mathrm{ag}}c_i}{4\pi\rho\left(r_{i+1}^3 - r_i^3\right)}\frac{1}{2}\left(r_{i+1}^2 - r_i^2\right) \tag{44}$$

where t is the thickness of the ITZ; ρ is the total number of the aggregate per unit volume, α, β, and κ are functions of the mean aggregate radius $\bar{R}$ and the mean square aggregate radius $\bar{R}^2$ according to the aggregate size distribution, c_i is the volume fraction of aggregates with radius ranging from r_i to r_{i+1}. Nu is the total number of zones (with radius ranging from r_i to r_{i+1}) used to characterize the aggregate size distribution. The volume fraction of the ITZ is finally obtained by the simple subtraction:

$$c_{\mathrm{itz}} = 1 - c_{\mathrm{ag}} - c_{\mathrm{bk}} - c_{fi}. \tag{45}$$

4 Stochastic micromechanical framework for the FRC

Based on the deterministic micromechanical framework in the above Section, the effective properties of the FRC can be estimated with the volume average or ensemble average of the descriptors for the microstructures. However, in real engineering problems, there is an inherent randomness of the specimen even under the same manufacturing process. To consider these fluctuations, the input of the micromechanical predicting model should be random [14–16]. Therefore, in this Section, the volume fraction and the material properties of the constituents in the multiphase composites are described by the appropriate random variables. Accordingly, our proposed micromechanical model is readily extended to a stochastic framework.

4.1 The stochastic descriptions for the microstructures of the FRC

Based on our proposed micromechanical model for the FRC, the uncertainties for the material's effective properties come from the fluctuations of the properties and the volume fractions of the different components. Meanwhile, the volume fractions of the ITZ and the bulk cement paste depend on the distribution of the aggregate and the thickness of the ITZ. Let $(\boldsymbol{\Omega}, \boldsymbol{\xi}, P)$ be a probability space, where $\boldsymbol{\Omega}$ is the sample space, $\boldsymbol{\xi}$ is the σ-algebra of subsets of $\boldsymbol{\Omega}$, and P is the probability measure, and $\mathbf{R}^N$ be an N-dimensional real vector space. Further, we define $E_{\mathrm{ag}}, \nu_{\mathrm{ag}}, E_{\mathrm{it}}, \nu_{\mathrm{it}}, E_{\mathrm{bk}}, \nu_{\mathrm{bk}}, E_{fi}, \nu_{fi}$ as the elastic modulus and the Poisson's ratio of the aggregate, the ITZ, the bulk cement paste, and the fibers, respectively. The sum of the volume fractions of the different components should be one, which means that the volume fractions of all the components are not independent. With the ITZ thickness, the volume fraction and the grading of the aggregate, the volume fractions of ITZ, and the bulk cement paste can be calculated by modifying the "void exclusion probability." Therefore, the random vector $\{E_{\mathrm{ag}}, \nu_{\mathrm{ag}}, E_{\mathrm{it}}, \nu_{\mathrm{it}}, E_{\mathrm{bk}}, \nu_{\mathrm{bk}}, E_{fi}, \nu_{fi}, c_{\mathrm{ag}}, t, \lambda_{fi}, c_{fi}, c_1, \cdots c_i \cdots c_{Nu}\}^T \in \mathbf{R}^{Nu+12}$ characterizes the uncertainties from all sources for the FRC based on our proposed micromechanical model.

4.2 The probabilistic characters of the material's properties

4.2.1 Monte Carlo simulation for the moments of the effective properties

By the stochastic descriptions of the microstructures, the effective properties of the FRC turn to a random function with the multivariate random variables based on our proposed deterministic micromechanical model. Hence, the effective modulus, such as K^*, μ^* or E^*, can be regarded as a random variable. The mean, the standard deviation, and the ith moment of the effective properties can be obtained using the Monte Carlo simulations as follows:

$$\mathrm{mean}(K^*) = \frac{1}{M}\sum_{m=1}^{M}(K_m^*), \quad \mathrm{imom}(K^*) = \frac{1}{M}\sum_{m=1}^{M}(K_m^*)^i, \tag{46}$$

$$\mathrm{mean}(\mu^*) = \frac{1}{M}\sum_{m=1}^{M}(\mu_m^*), \quad \mathrm{imom}(\mu^*) = \frac{1}{M}\sum_{m=1}^{M}(\mu_m^*)^i, \tag{47}$$

$$\mathrm{mean}(E^*) = \frac{1}{M}\sum_{m=1}^{M}(E_m^*), \quad \mathrm{imom}(E^*) = \frac{1}{M}\sum_{m=1}^{M}(E_m^*)^i \tag{48}$$

where M is the sample size; mean ( ) and imom ( ) denote the mean and the i-order moment, respectively; K_m^*, μ_m^*, and E_m^* are the mth sample of the effective bulk modulus, the shear modulus, and Young's modulus.

4.2.2 The maximum entropy distribution for the effective properties

It is noted that the moment matrix in Eq. (6) usually becomes singular, when the number of parameters becomes large. To obtain more stable results, the normalization procedures are adopted herein for the effective properties. Therefore, the i-order moments for the normalized effective properties are reached as below:

$$\bar{m}_i(K^*) = \frac{1}{M}\left(\sum_{m=1}^{M}\left(\frac{K_m^* - \text{mean}(K^*)}{\text{sd}(K^*)}\right)^i\right), \text{sd}(K^*) = \sqrt{\left(\frac{1}{M}\sum_{m=1}^{M}\left(K_m^* - \text{mean}(K^*)\right)^2\right)^{1/2}}, \quad (49)$$

$$\bar{m}_i(\mu^*) = \frac{1}{M}\left(\sum_{m=1}^{M}\left(\frac{\mu_m^* - \text{mean}(\mu^*)}{\text{sd}(\mu^*)}\right)^i\right), \text{sd}(\mu^*) = \sqrt{\left(\frac{1}{M}\sum_{m=1}^{M}\left(\mu_m^* - \text{mean}(\mu^*)\right)^2\right)^{1/2}}, \quad (50)$$

$$\bar{m}_i(E^*) = \frac{1}{M}\left(\sum_{m=1}^{M}\left(\frac{E_m^* - \text{mean}(E^*)}{\text{sd}(E^*)}\right)^i\right), \text{sd}(E^*) = \sqrt{\left(\frac{1}{M}\sum_{m=1}^{M}\left(E_m^* - \text{mean}(E^*)\right)^2\right)^{1/2}} \quad (51)$$

where sd ( ) and $\bar{m}_i$ denote the standard deviation and i-order moment for the normalized properties, respectively. The pdf of the normalized effective properties $\bar{f}(\bar{x})$ can be reached by solving the following equations:

$$\begin{bmatrix} 1 & 0 & \cdots & \bar{m}_{n-1} \\ 0 & 1 & \cdots & \bar{m}_n \\ \vdots & \vdots & \ddots & \vdots \\ \bar{m}_{n-1} & \bar{m}_n & \cdots & \bar{m}_{2(n-1)} \end{bmatrix} \begin{Bmatrix} \bar{a}_1 \\ 2\bar{a}_2 \\ \vdots \\ n\bar{a}_n \end{Bmatrix} = \begin{Bmatrix} 0 \\ -1 \\ \vdots \\ -(n-1)\bar{m}_{n-2} \end{Bmatrix}, \quad (52)$$

$$\bar{a}_0 = \ln\left(\frac{1}{\int_{-\infty}^{+\infty} e^{\bar{a}_1 x + \bar{a}_2 x^2 + \cdots \bar{a}_n x^n} \mathrm{d}x}\right) \quad (53)$$

where $\bar{a}_i, i = 0, 1, 2 \ldots n$ are the coefficients for the normalized effective properties. With the $\bar{f}(\bar{x})$, the pdf $f(x)$ of the effective properties can be obtained as follows:

$$f_K(x) = \frac{1}{sd(K^*)}\bar{f}\left(\frac{x - \text{mean}(K^*)}{\text{sd}(K^*)}\right), \quad (54)$$

$$f_\mu(x) = \frac{1}{\text{sd}(\mu^*)}\bar{f}\left(\frac{x - \text{mean}(\mu^*)}{\text{sd}(\mu^*)}\right), \quad (55)$$

$$f_E(x) = \frac{1}{\text{sd}(E^*)}\bar{f}\left(\frac{x - \text{mean}(E^*)}{sd(E^*)}\right) \quad (56)$$

where $f_K(x)$, $f_\mu(x)$, and $f_E(x)$ are the pdfs for the effective bulk modulus, shear modulus, and Young's modulus.

From the above, to obtain the pdfs of the effective properties of the FRC, the following computational procedures are employed: Firstly, the random vector $\{E_{ag}, \nu_{ag}, E_{it}, \nu_{it}, E_{bk}, \nu_{bk}, E_{fi}, \nu_{fi}, c_{ag}, t, \lambda_{fi}, c_{fi}, c_1, \ldots c_i \ldots c_{Nu}\}^T$ is formed according to the distributions of the different random variables. Secondly, with each random vector, the sample for the effective properties of the FRC can be reached with the deterministic micromechanical framework using Eqs. (8)–(45). Thirdly, the different order moments can be calculated with the samples of the effective properties of the FRC with Eqs. (46)–(48). Finally, the pdfs can be reached with the different order moments according to Eqs. (49)–(56).

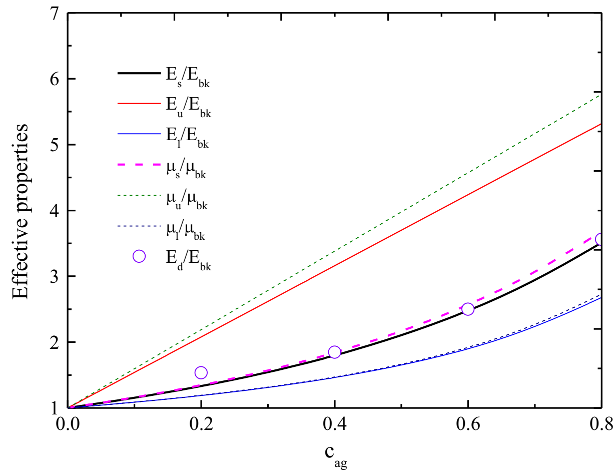

Fig. 3 Comparisons among our predictions, the existing micromechanical results, and the experimental data for the properties of concrete [60]. Here c_{ag} is the volume fraction of the aggregates; E_d and E_{bk} (μ_{bk}) is the experimental data of concrete Young's modulus and the Young's modulus (shear modulus) of bulk cement paste, respectively; E_s, E_u, and E_l (μ_s, μ_u, and μ_l) are the results herein, upper bounds, and lower bounds for Young's modulus (shear modulus)

5 Verifications

5.1 Verifications for the deterministic micromechanical framework

The experimental data combined with the existing micromechanical models are employed to verify our proposed deterministic micromechanical framework.

The predictions after the first and the second-level homogenizations, which are the estimations for the properties of the concrete made up of the aggregate, the ITZ, and the cement paste, are compared with the Voigt upper bounds and the Reuss lower bounds combined with the experimental data of [60]. As exhibited by Fig. 3, the predictions of Young's modulus herein correspond well with the experimental data obtained by Stock et al. [60]. Meanwhile, the predictions of Young's modulus and the shear modulus lie reasonably between the corresponding Voigt upper bounds and the Reuss lower bounds, which implies that our proposed deterministic micromechanical framework for the FRC can predict the properties of the concrete.

The predictions after the third-level homogenizations, which are the estimations for the properties of the FRC, are compared with the experimental data of [3]. Two types of the different shapes (with $\gamma = 5$ and $\gamma = 50$) are considered in this example. Figure 4 shows the comparisons between our predictions and the experimental data for the properties of the FRC. It can be found from Fig. 4 that our predicted results meet well with the experimental data when different types of concrete matrix are considered. Since the volume fraction of the steel fiber is low in this case, which varies from 0 to 1.5%, the influence of the fiber shape on the properties of the FRC is not significant. By changing the volume fraction of the steel fiber from 0 to 5%, it can be observed from Fig. 5a that with the increase in the aspect ratios the FRC shows larger Young's modulus. However, there is no meaningful difference between the FRC properties for $\gamma = 50$ and $\gamma = 100$. Similar conclusions can be reached for the shear modulus, as displayed in Fig. 5b.

5.2 Verifications for the stochastic micromechanical framework

The stochastic micromechanical framework is consisting of the stochastic descriptions of the material microstructures, the deterministic micromechanical model, and the maximum entropy-based simulation program. The commonly used probability density functions and the direct Monte Carlo simulations are utilized to verify the proposed stochastic micromechanical framework for the FRC.

The probability distribution of the FRC properties is important for the structure reliability analysis. The commonly used distributions, such as the normal distribution, the lognormal distribution, and the Weibull distribution, are employed to approximate the real distribution of the material's properties with certain prior assumptions. Figure 6 shows the comparisons among the results of our proposed distribution-free method

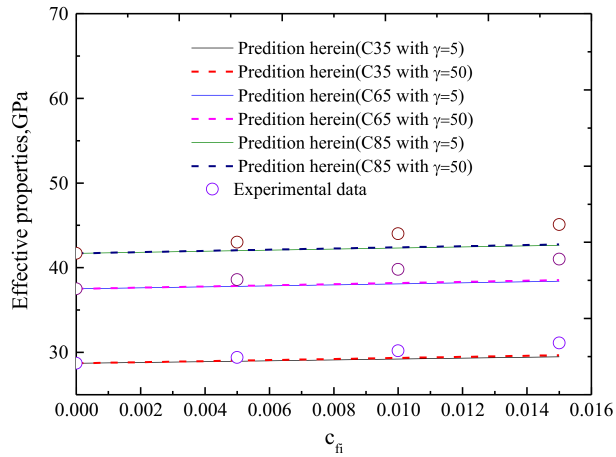

Fig. 4 Comparisons among our predictions, the existing micromechanical results, and the experimental data [3]

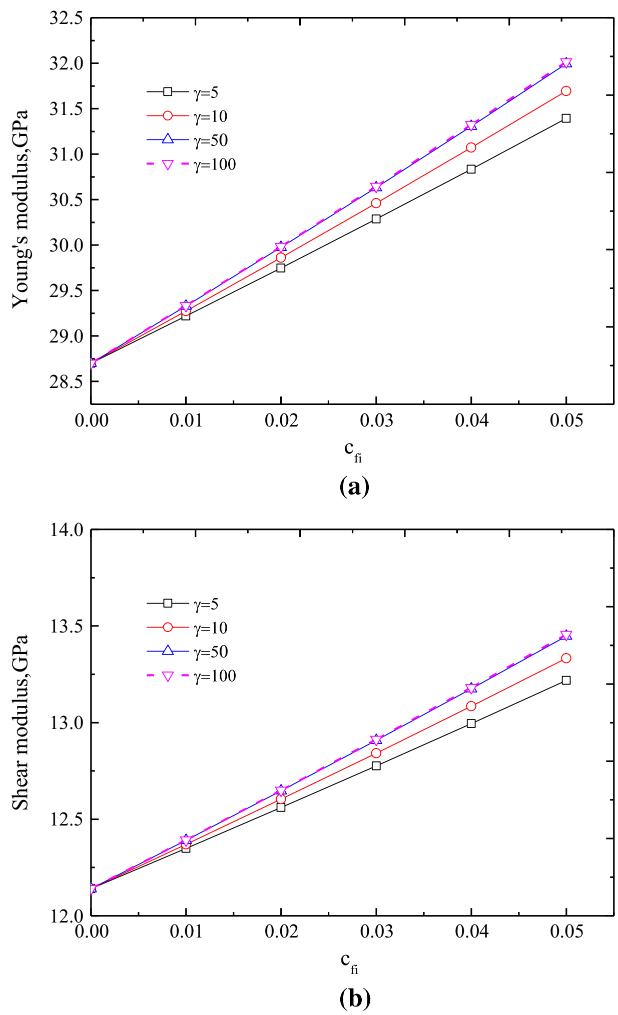

Fig. 5 Influence of the fiber shapes on the properties of the FRC. **a** Young's modulus. **b** Shear modulus

and the theoretical solutions of the commonly used pdfs. From Fig. 6a, it can be found that the maximum entropy-based pdf can approximate the normal distributions with different distribution parameters (including the mean and the standard deviations). Meanwhile, the approximations become better with the increase in the

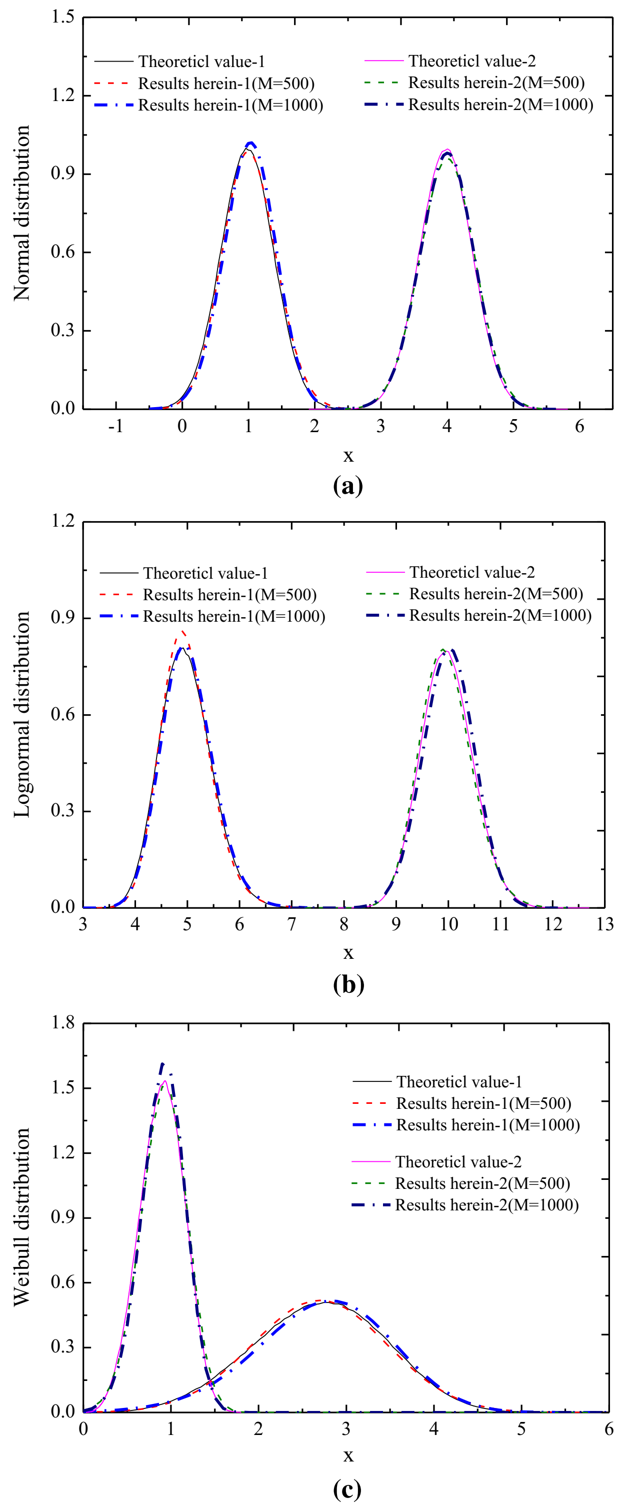

Fig. 6 Comparisons among our predictions and commonly used pdfs for concrete material. **a** Normal distribution, with $f(x) = \frac{1}{\sigma\sqrt{2\pi}} e^{-\frac{(x-\mu)^2}{2\sigma^2}}$ (-1 means $\mu = 1, \sigma = 0.4$, -2 means $\mu = 4, \sigma = 0.4$). **b** Lognormal distribution, with $f(x) = \frac{1}{x\sigma\sqrt{2\pi}} e^{-\frac{(\ln x-\mu)^2}{2\sigma^2}}$ (-1 means $\mu = 1$, $\sigma = 0.5$, -2 means $\mu = 10$, $\sigma = 0.5$). **c** Weibull distribution, with $f(x) = \begin{cases} \frac{k}{\lambda}\left(\frac{x}{\lambda}\right)^{k-1} e^{-(x/\lambda)^k} & x \geq 0 \\ 0 & x < 0 \end{cases}$ (-1 means $\lambda = 1, k = 4$, -2 means $\lambda = 3, k = 4$)

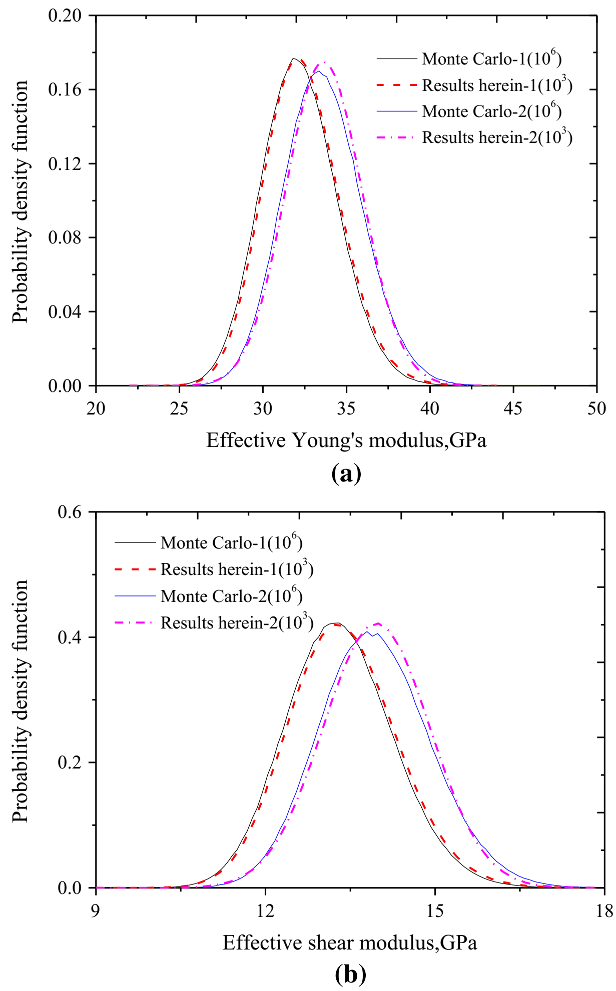

Fig. 7 Comparisons among our predictions and direct Monte Carlo simulations using varied ITZs where − 1 and − 2 represent type I (mean of ITZ thickness = 0.01 mm)and type II ITZ (mean of ITZ thickness = 0.03 mm), respectively. **a** Young's modulus. **b** Shear modulus

sample size. The maximum entropy-based pdf meets well with the theoretical value with 10^3 sample points. As to the lognormal distribution and the Weibull distributions, similar conclusions can be reached from Fig. 6b, c, which implies that our proposed maximum entropy distributions are capable of representing these distributions without any premise. It is noted that the fourth-order moments are adopted in our simulation framework herein.

The numerical examples are adopted to verify the stochastic micromechanical framework which can consider the effects of both ITZ and fibers with different shapes. The grading of the aggregate and the mean values for the properties of the aggregate, the ITZ and the bulk cement paste are based on the previous work of Stock et al. [60]. The mean values for the properties of different fibers are from [10].The lognormal distribution is utilized to represent the pdfs of the constituents' properties. The volume fractions of the aggregate and the fiber are assumed to follow the Beta distribution with the mean values as 60 and 4%, respectively. The coefficients of variation for all the random variables are supposed to be 0.1 in the following stochastic modeling examples.

Figure 7 shows the comparisons among our predictions and the results of the direct Monte carlo simulations for the pdfs of the SFRC's properties with two types of ITZ thicknesses (which are supposed to follow the normal distribution with 0.01 and 0.03 mm as the mean value). It can be observed that our predictions are close to the results of direct Monte Carlo simulations when different ITZs are considered. Meanwhile, with the increase in the mean value of ITZ, the FRC demonstrates lower properties statistically.

Figure 8 displays the comparisons among results herein and those of direct Monte Carlo simulations for the properties of SFRC and polypropylene fiber-reinforced concrete (PFRC). No matter what type of fiber is

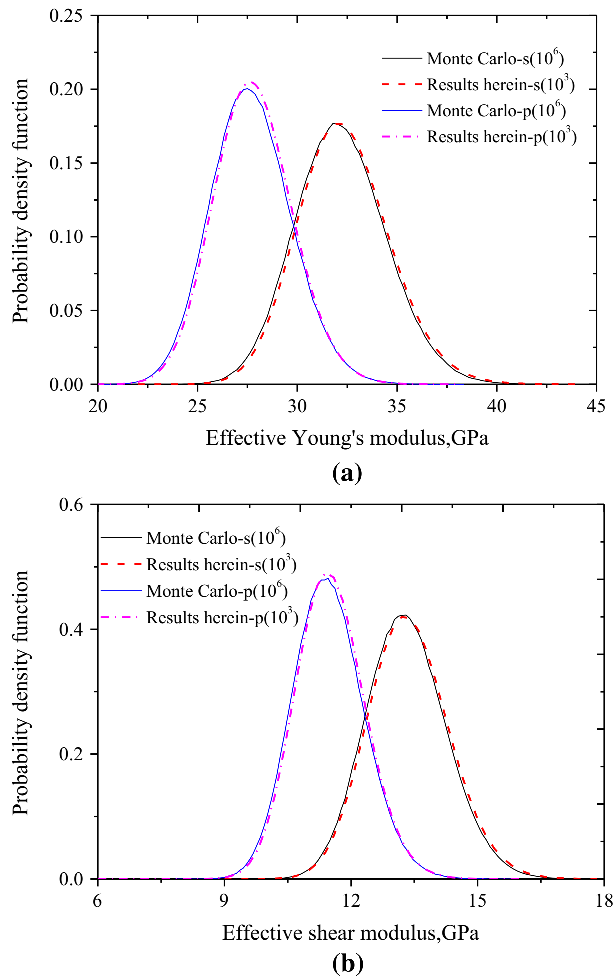

Fig. 8 Comparisons among our predictions and direct Monte Carlo simulations using different fibers, where $-s$ and $-p$ represent steel fiber- and polypropylene fiber-reinforced concrete, respectively. **a** Young's modulus. **b** Shear modulus

considered, our predictions are all close to those obtained by the direct Monte Carlo simulations. Meanwhile, the SFRC demonstrates larger properties statistically than PFRC.

Figure 9 exhibits the comparisons among results herein and those of direct Monte Carlo simulations for the effective properties of SFRC with different shapes. Similarly, the pdfs for the effective Young's modulus and shear modulus obtained using the proposed framework are close to the results of the direct Monte Carlo simulations. In addition, with the increase in mean values for the aspect ratios, the SFRC have larger effective properties statistically.

It should be mentioned that the iterative times in solving the micromechanical equations by direct Monte carlo method are 10^6 times. However, the iterative times in our numerical computing can be dramatically reduced to 10^3 times. The direct Monte Carlo simulation results for the pdfs are reached with the histograms of the 10^6 samples of the effective properties. Nevertheless, the pdfs herein are obtained with the different order moments calculated by using 10^3 samples of the effective properties based on the maximum entropy principle.

6 Conclusions

The current micromechanical models for FRC are mainly based on the deterministic framework, and very few models can consider the effects of both the ITZ and the fiber shapes together. In this paper, a stochastic micromechanical framework is proposed for predicting the FRC's probabilistic properties. The FRC is represented as a multiphase composite composed of the aggregate, the interfacial transition zone, the bulk

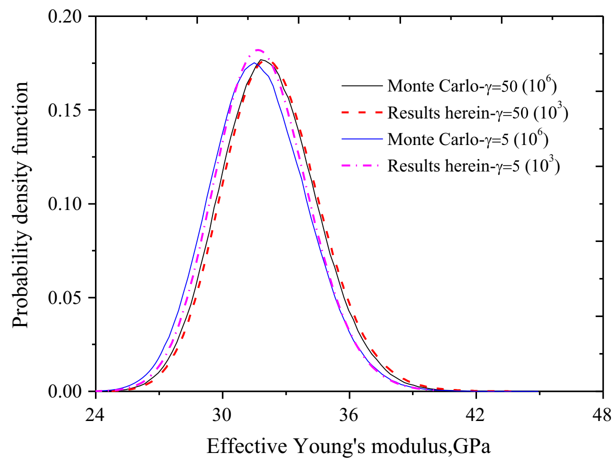

(a)

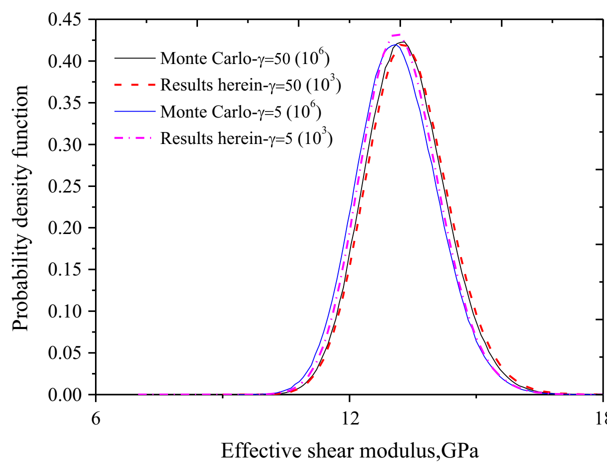

(b)

Fig. 9 Comparisons among our predictions and direct Monte Carlo simulations using fibers with different shapes. **a** Young's modulus. **b** Shear modulus

cement paste, and the fibers. Based on the "void exclusion probability," the volume fractions of the ITZ and the bulk cement paste are analytically calculated. Multilevel homogenization schemes are presented to predict the material's effective properties considering the effects of aggregate, the ITZ, and the fibers with different shapes. The stochastic micromechanical framework is reached by modeling the volume fractions and properties of the constituents as stochastic. The maximum entropy distribution is modified to estimate the probability density function of the material's properties using their different order moments. Numerical simulations are performed to verify our proposed deterministic and stochastic micromechanical framework. From this study, the following conclusions can be drawn:

(i) The proposed stochastic micromechanical framework is capable of predicting the FRC's probabilistic behaviors considering the effects of the ITZ and the fibers with different shapes.
(ii) The presented maximum entropy-based simulation framework is accurate and computationally efficient in characterizing the FRC's effective properties compared with the direct Monte Carlo simulation. In addition, it can approximate the commonly used pdfs without any premises.
(iii) With the increase in aspect ratio or properties of fibers, the FRC demonstrates larger properties. However, when the mean values of ITZ thicknesses increase, the effective properties of FRC decrease statistically.

Acknowledgements This work is supported by the National Natural Science Foundation of China (51508404, 51478348, 51278360, 51308407, U1534207). This work is also supported by the National Key Basic Research and Development Program (973 Program, No. 2011CB013800), State Key Laboratory of High Performance Civil Engineering Materials (No. 2015CEM008), Program of Shanghai Science and Technology Commission(15DZ1205003), the 1000 Talents Plan Short-Term Program by the Organization Department of the Central Committee of the CPC, Research Program of State Key Laboratory for Disaster Reduction in Civil Engineering, the Funds of Fundamental Research Plan for the Central Universities.

Compliance with ethical standards

Conflict of interest The authors declare that they have no conflict of interest.

References

1. Mohammadi, Y., Carkon-Azad, R., Singh, S.P., Kaushik, S.K.: Impact resistance of steel fibrous concrete containing fibres of mixed aspect ratio. Constr. Build. Mater. **23**, 183–189 (2009)
2. Yan, Z.G., Zhu, H.H., Ju, J.W.: Behavior of reinforced concrete and steel fiber reinforced concrete shield TBM tunnel linings exposed to high temperatures. Constr. Build. Mater. **38**, 610–618 (2013)
3. Thomas, J., Ramaswamy, A.: Mechanical properties of steel fiber-reinforced concrete. J. Mater. Civ. Eng. **19**, 385–392 (2007)
4. Tan, K.H., Paramasivam, P., Tan, K.C.: Instantaneous and long-term deflections of steel fiber reinforced concrete beams. ACI Struct. J. **91**, 384–393 (1994)
5. Ashour, S.A., Wafa, F.F., Kamal, M.I.: Effect of concrete compressive strength and tensile reinforcement ratio on the flexural behavior of fibruous concrete beams. Eng. Struct. **22**, 1145–1158 (2000)
6. Ezeldin, A.S., Balagaru, P.N.: Normal and high strength fiber reinforced concrete under compression. J. Mater. Civil. Eng. **4**, 415–429 (1992)
7. Mansur, M.A., Chin, M.S., Wee, T.H.: Stress–strain relationship of high strength fiber concrete in compression. J. Mater. Civil. Eng. **11**, 21–29 (1999)
8. Ahmad, H.A., Lagoudas, C.L.: Effective elastic properties of fiber-reinforced concrete with random fibers. J. Eng. Mech. **117**, 2931–2938 (1991)
9. Yan, Z.G., Shen, Y., Zhu, H.H., Lu, Y., Li, X.J.: Experimental investigation of reinforced concrete and hybrid fiber reinforced concrete shield tunnel segments subjected to elevated temperature. Fire Saf. J. **71**, 86–99 (2015)
10. Dutra, V.F.P., Maghous, S., Filho, A.C., Pacheco, A.R.: A micromechanical approach to elastic and viscoelastic properties of fiber reinforced concrete. Cem. Concr. Res. **40**, 460–472 (2010)
11. Teng, T.L., Chu, Y.A., Chang, F.A., Chin, H.S.: Calculating the elastic moduli of steel fiber reinforced concrete using a dedicated empirical formula. Comput. Mater. Sci. **31**, 337–346 (2004)
12. Gal, E., Kryvoruk, R.: Meso-scale analysis of FRC using a two-step homogenization approach. Comput. Struct. **89**, 921–929 (2011)
13. Guan, X.F., Liu, X., Jia, X., Yuan, Y., Cui, J.Z., Mang, H.A.: A stochastic multiscale model for predicting mechanical properties of fiber reinforced concrete. Int. J. Solids Struct. **56–57**, 280–289 (2015)
14. Ferrante, F., Graham-Brady, L.: Stochastic simulation of non-Gaussian/non-stationary properties in a functionally graded plate. Comput. Methods Appl. Mech. Eng. **194**, 1675–1692 (2005)
15. Chen, Q., Zhu, H.H., Ju, J.W., Guo, F., Wang, L.B., Yan, Z.G., Deng, T., Zhou, S.: A stochastic micromechanical model for multiphase composite containing spherical inhomogeneities. Acta Mech. **226**(6), 1861–1880 (2015)
16. Zhu, H.H., Chen, Q., Ju, J.W., Yan, Z.G., Guo, F., Wang, Y.Q., Jiang, Z.W., Zhou, S., Wu, B.: Maximum entropy based stochastic micromechanical model for a two-phase composite considering the inter-particle interaction effect. Acta Mech. **226**(9), 3069–3084 (2015)
17. Ferrante, F.J., Brady, L.L.G., Acton, K., Arwade, S.R.: An overview of micromechanics-based techniques for the analysis of microstructural randomness in functionally graded materials. AIP Conf. Proc. **973**, 190–195 (2008)
18. Rahman, S., Chakraborty, A.: A stochastic micromechanical model for elastic properties of functionally graded materials. Mech. Mater. **39**, 548–563 (2007)
19. Bai, X.P., Liu, Y.N.: Reliability analysis on civil engineering project based on integrated adaptive simulation annealing and gray correlation method. Front. Struct. Civ. Eng. **10**(4), 462–471 (2016)
20. Guan, X.F., Yu, H.T., Tian, X.: A stochastic second-order and two-scale thermo-mechanical model for strength prediction of concrete materials. Int. J. Numer. Methods Eng. **108**(8), 885–901 (2016)
21. Guan, X.F., Li, M.X., He, W.M., Jiang, Z.W.: Some superconvergence results of high-degree finite element method for a second order elliptic equation with variable coefficients. Cent. Eur. J. Math. **12**(11), 1733–1747 (2014)
22. Chen, Q., Zhu, H.H., Ju, J.W., Jiang, Z.W., Yan, Z.G., Li, H.X.: Stochastic micromechanical predictions for the effective properties of concrete considering the interfacial transition zone effects. Int. J. Damage Mech. (2017). https://doi.org/10.1177/1056789517728501
23. Jaynes, E.T.: Information theory and statistical mechanics. Phys. Rev. **106**, 620–630 (1957)
24. Li, X.J., Zuo, Y.L., Zhuang, X.Y., Zhu, H.H.: Estimation of fracture trace length distributions using probability weighted moments and L-moments. Eng. Geol. **168**, 69–85 (2014)
25. Bernard, O., Ulm, F.J., Lemarchand, E.: A multiscale micromechanics-hydration model for the early-age elastic properties of cement-based materials. Cem. Concr. Res. **33**, 1293–1309 (2003)
26. Constantinides, G., Ulm, F.J.: The effect of two types of C–S–H on the elasticity of cement-based materials: results from nanoindentation and micromechanical modeling. Cem. Concr. Res. **34**(1), 67–80 (2004)
27. Zheng, J.J., Wong, H.S., Buenfeld, N.R.: Assessing the influence of ITZ on the steady-state chloride diffusivity of concrete using a numerical model. Cem. Concr. Res. **39**, 805–813 (2009)
28. Zheng, J.J., Zhou, X.Z., Jin, X.Y.: An n-layered spherical inclusion model for predicting the elastic moduli of concrete with inhomogeneous ITZ. Cem. Concr. Compos. **34**, 716–723 (2012)
29. Dridi, W.: Analysis of effective diffusivity of cement based materials by multi-scale modelling. Mater. Struct. **46**, 313–326 (2013)

30. Gao, X., Wei, Y., Huang, W.: Critical aspects of scanning probe microscope mapping when applied to cement pastes. Adv. Cem. Res. (2018). https://doi.org/10.1680/jadcr.17.00093
31. Ju, J.W., Chen, T.M.: Micromechanics and effective moduli of elastic composites containing randomly dispersed ellipsoidal inhomogeneities. Acta Mech. **103**, 103–121 (1994)
32. Ju, J.W., Chen, T.M.: Effective elastic moduli of two-phase composites containing randomly dispersed spherical inhomogeneities. Acta Mech. **103**, 123–144 (1994)
33. Ju, J.W., Zhang, X.D.: Micromechanics and effective transverse elastic moduli of composites with randomly located aligned circular fibers. Int. J. Solids Struct. **35**(9–10), 941–960 (1998)
34. Ju, J.W., Sun, L.Z.: A novel formulation for the exterior-point Eshelby's tensor of an ellipsoidal inclusion. J. Appl. Mech. **66**(2), 570–574 (1999)
35. Ju, J.W., Sun, L.Z.: Effective elastoplastic behavior of metal matrix composites containing randomly located aligned spheroidal inhomogeneities. Part I: micromechanics-based formulation. Int. J. Solids Struct. **38**(2), 183–201 (2001)
36. Sun, L.Z., Ju, J.W.: Effective elastoplastic behavior of metal matrix composites containing randomly located aligned spheroidal inhomogeneities. Part II: applications. Int. J. Solids Struct. **38**(2), 203–225 (2001)
37. Sun, L.Z., Ju, J.W.: Elastoplastic modeling of metal matrix composites containing randomly located and oriented spheroidal particles. J. Appl. Mech. **71**, 774–785 (2004)
38. Ju, J.W., Yanase, K.: Micromechanics and effective elastic moduli of particle-reinforced composites with near-field particle interactions. Acta Mech. **215**(1), 135–153 (2010)
39. Ju, J.W., Yanase, K.: Micromechanical effective elastic moduli of continuous fiber-reinforced composites with near-field fiber interactions. Acta Mech. **216**(1), 87–103 (2011)
40. Yanase, K., Ju, J.W.: Effective elastic moduli of spherical particle reinforced composites containing imperfect interfaces. Int. J. Damage Mech. **21**(1), 97–127 (2012)
41. Zhu, H.H., Chen, Q., Yan, Z.G., Ju, J.W., Zhou, S.: Micromechanical model for saturated concrete repaired by electrochemical deposition method. Mater. Struct. **47**, 1067–1082 (2014)
42. Yan, Z.G., Chen, Q., Zhu, H.H., Ju, J.W., Zhou, S., Jiang, Z.W.: A multiphase micromechanical model for unsaturated concrete repaired by electrochemical deposition method. Int. J. Solids Struct. **50**(24), 3875–3885 (2013)
43. Chen, Q., Zhu, H.H., Yan, Z.G., Deng, T., Zhou, S.: Micro-scale description of the saturated concrete repaired by electrochemical deposition method based on Mori-Tanaka method. J. Build. Struct. **36**(1), 98–103 (2015)
44. Chen, Q., Zhu, H.H., Yan, Z.G., Ju, J.W., Deng, T., Zhou, S.: Micro-scale description of the saturated concrete repaired by electrochemical deposition method based on self-consistent method. Chin. J. Theor. Appl. Mech. **47**(2), 367–371 (2015)
45. Chen, Q., Zhu, H.H., Yan, Z.G., Ju, J.W., Jiang, Z.W., Wang, Y.Q.: A multiphase micromechanical model for hybrid fiber reinforced concrete considering the aggregate and ITZ effects. Constr. Build. Mater. **114**, 839–850 (2016)
46. Chen, Q., Nezhad, M.M., Fisher, Q., Zhu, H.H.: Multi-scale approach for modeling the transversely isotropic elastic properties of shale considering multi-inclusions and interfacial transition zone. Int. J. Rock Mech. Min. Sci. **84**, 95–104 (2016)
47. Chen, Q., Jiang, Z.W., Yang, Z.H., Zhu, H.H., Ju, J.W., Yan, Z.G., Wang, Y.Q.: Differential-scheme based micromechanical framework for saturated concrete repaired by the electrochemical deposition method. Mater. Struct. **49**(12), 5183–5193 (2016)
48. Chen, Q., Jiang, Z.W., Zhu, H.H., Ju, J.W., Yan, Z.G.: An improved micromechanical framework for saturated concrete repaired by the electrochemical deposition method considering the imperfect bonding. J. Eng. **3**, 1–11 (2016)
49. Chen, Q., Jiang, Z.W., Zhu, H.H., Ju, J.W., Yan, Z.G.: Micromechanical framework for saturated concrete repaired by the electrochemical deposition method with interfacial transition zone effects. Int. J. Damage Mech. **26**(2), 210–228 (2017)
50. Chen, Q., Jiang, Z.W., Yang, Z.H., Zhu, H.H., Ju, J.W., Yan, Z.G., Wang, Y.Q.: Differential-scheme based micromechanical framework for unsaturated concrete repaired by the electrochemical deposition method. Acta Mech. **228**(2), 415–431 (2017)
51. Nezhad, M.M., Zhu, H.H., Ju, J.W., Chen, Q.: A simplified multiscale damage model for the transversely isotropic shale rocks under tensile loading. Int. J. Damage Mech. **25**(5), 705–726 (2016)
52. Hong, S., Yuan, K.Y., Ju, J.W.: Initial strain energy-based thermo-elastoviscoplastic two-parameter damage-self-healing models for bituminous composites-Part I: Formulations. Int. J. Damage Mech. **25**(8), 1082–1102 (2016)
53. Hong, S., Yuan, K.Y., Ju, J.W.: Initial strain energy-based thermo-elastoviscoplastic two-parameter damage-self-healing models for bituminous composites-Part II: Computational aspects. Int. J. Damage Mech. **25**(8), 1103–1129 (2016)
54. Ju, J.W., Wu, Y.: Stochastic micromechanical damage modeling of progressive fiber breakage for longitudinal fiber-reinforced composites. Int. J. Damage Mech. **25**(2), 203–227 (2016)
55. Smith, J.C.: Correction and extension of Van der Poel's method for calculating the shear modulus of a particulate composite. J. Res. Natl Bureau Stand A Phys. Chem. **78**(3), 355–361 (1974)
56. Smith, J.C.: Simplification of Van der Poel's formula for the shear modulus of a particulate composite. J. Res. Natl Bureau Stand A Phys. Chem. **79A**(2), 419–423 (1975)
57. Berryman, J.G.: Long-wave propagation in composite elastic media II. Ellipsoidal inclusion. J. Acoust. Soc. Am. **68**(6), 1820–1831 (1980)
58. Ej, G., Bentz, D.P.: Analytical formulas for interfacial transition zone properties. Adv. Cem. Based Mater. **6**(3–4), 99–108 (1997)
59. Lu, B.L., Torquato, S.: Nearest-surface distribution functions for polydispersed particle system. Phys. Rev. A **45**(8), 5530–5544 (1992)
60. Stock, A.F., Hannant, D.J., Williams, R.I.T.: The effect of aggregate concentration upon the strength and modulus of elasticity of concrete. Mag. Concr. Res. **31**(109), 225–34 (1979)